(Received 12 July 2024, Accepted 29 August 2024, Scheduled 11 September 2024)

Transmission Characterization of Four-Layer PCB Differential Lines Based on Modified Kron's Methodology

Weibing Xiao[1,2], Kuangang Fan[1,2], Fazhu Zhou[1,2,*], Jizan Zhu[1,2], and Shuliang Li[1,2]

[1] *The School of Electrical Engineering and Automation, Jiangxi University of Science and Technology, China*
[2] *The Key Laboratory of Magnetic Levitation Technology, Jiangxi University of Science and Technology, China*

ABSTRACT: This paper addresses the high-frequency signal transmission problem of high-speed differential lines on four-layer printed circuit boards (PCBs). It establishes a mathematical model of high-speed differential lines in conjunction with modified Kron's methodology (MKM), a nontraditional circuit modeling method. The article builds the model through diakoptics of differential lines, then generates the corresponding topology maps, and finally creates the model through tensorial analysis of the network (TAN). The differential line model is simulated and optimized by HFSS. This paper mainly analyzes the influence of differential line spacing and grounding vias on the signal transmission of differential lines. Secondly, it analyzes the problem of multi-group differential line arrangement based on the above work. Finally, the experimental results obtained are consistent with the simulation ones.

1. INTRODUCTION

As 5G and 6G technologies advance, permanent magnetic levitation (PML) trains are emerging as the most attractive urban transportation system. However, stable PML data transmission requires both rapid and steady signals as well as long-lasting hardware solutions. The data acquisition of the PML train through PCB and 5G signals is shown in Fig. 1. The key components of the PML train control and acquisition are the PCB and integrated circuit (IC) chip, and the most basic bridge between the chip and the PCB is microstrip line. There are transmission lines on the power and ground layers in the PCB, and the transmission lines of the two layers are connected through vias [1, 2]. Nonetheless, PML faces difficulties as the signal integrity (SI) and electromagnetic compatibility (EMC) of PCB are constantly challenged by the increase in signal transmission frequency [3–6]. The transmission line analysis and design on the PCB needs to be further refined to overcome this difficulty [7].

SI requires more precise system-level analysis when the frequency of the signal transmission rises. Typically, this investigation involves power supply, signal modeling, and simulation. A coupling effect happens between the differential lines during high-frequency differential signal transmission, which has an impact on the signal's accurate transmission. As a result, issues with conduction and radiation could arise [8, 9]. Crosstalk, which results in electromagnetic interference (EMI)/EMC issues, is the noise produced by the coupling, mutual capacitance, and mutual inductance between two signal lines. The higher the signal frequency is, the closer the distance is between the differential line excitation sources, and the more pronounced the coupling effect is. Moreover, the characteristic impedance matching is complicated by the discontinuous phenomena brought about by the via and pad, which makes the signal transmission considerably more irregular and the transmission loss worse [10, 11]. The design and modeling of high-speed PCB differential lines will be probably more complicated in the future.

FIGURE 1. PML transfer data.

High-speed PCBs have been studied by numerous researchers; however, they still have certain drawbacks. Initially, lengthy processing periods are needed for techniques like the method of the moment [12], finite difference time domain [13], finite element method (FEM) [14], and finite integration time domain. Second, the necessary speed and precision cannot yet be reached by 1D, 2D, or 2.5D processing. By using tests, Baek et al. proposed a difference-line equivalent circuit model, which is also appropriate for differential mode

* Corresponding author: Fazhu Zhou (411768620@qq.com).

and common mode [15]. However, the conversions mentioned in this method need to be good between the erase partition signals to be valid when being coupled, and the calculation process is complex. On the other hand, MKM is a high-speed PCB calculating technique that is accurate, quick, and very flexible, and it has been shown to be effective and precise [16].

To the best of the authors' knowledge, very few MKMs are currently in use, and only a relatively small number of researchers modelled high-speed differential lines based on this method. This study's unique contribution is the MKM modeling of high-speed difference lines.

There are five sections to this study. The pertinent history and development conditions are introduced in Section 1. Section 2 talks about MKM modeling. Section 3 shows a among between HFSS simulations, VAN experiments, and MKM-based mathematical model data. Section 4 discusses Section 3 and analyzes the effect of parameters on the transmission characteristics of differential lines, and Section 5 summarizes the conclusions drawn in this paper.

2. KRON'S MODEL AND PCB MODELING METHOD

2.1. Introduction to TAN

Gabriel Kron wrote the first manual on non-traditional circuit formalism for TAN in 1940. The original purpose of this textbook was to teach the general theory of motors. Several further TAN applications in electrical engineering were also established ten years later [17]. Mesh splitting analysis, or the original network notion, is linked to TAN by Kron [18]. This allows for the study of both simple and complicated engineering systems. The initial network analysis is a two-step process that is commonly used to describe complicated engineering challenges. To address each component of the problem independently, the problem is first broken down into smaller parts. Next, identify an adaptable mathematical theory that integrates all components to yield the anticipated outcomes.

The benefits of TAN over the conventional Kirchhoff's node method and grid approach are as follows:

1. There is integration of the electrical-electromagnetic coupling effects between electronic components.
2. It is possible to compute electrical parameters in systems that have multidimensional physical interactions.
3. Use a less complicated tensor checking technique to analyze intricate electronic systems.

Firstly, the complex problem can be solved by an equivalent circuit topology diagram, which systematically describes the problem, taking into account the basic principles of each element of the structure to be studied. Secondly, the topological graph of a complex structure is transformed into a tensor mathematical expression. Finally, an equivalent mathematical model is developed by combining the tensor mathematical expressions [19–23].

2.2. PCB Modeling Process

The use of MKM to differential line modeling is covered in detail in this section. But to show how the enhanced Green's

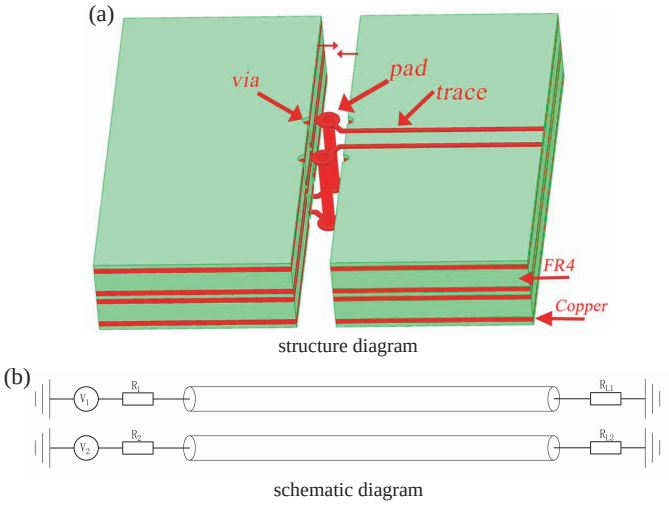

FIGURE 2. Differential lines on a four-layer PCB board.

method modeling is to create a mathematical model, this paper examines a straightforward four-layer plate structure as a feasibility study [24–27]. Fig. 2 shows the external input impedance as differential excitation signals. A critical component of studying high-speed differential lines is characteristic impedance matching.

When the microstrip line is between air and medium, and $0.127 < wid < 0.381$ mm, its characteristic impedance (Z_C) model, the related Z_C, capacitance (C), and inductance (L) can be calculated by the following formulas, and that In is the natural logarithm in the formulas appearing below:

$$Z_C = \frac{89}{\sqrt{\varepsilon_r + 1.41}} \mathrm{In}\left(\frac{5.98h}{0.8wid + t}\right) \tag{1}$$

$$\upsilon = \frac{\upsilon_0}{\sqrt{\varepsilon_r}} \tag{2}$$

$$L = \frac{Z_C l}{\upsilon} \tag{3}$$

$$C = \frac{l}{\upsilon Z_C} \tag{4}$$

where ε_r is the relative dielectric constant; υ_0 is the speed of vacuum light; wid, l, t are the width, length, and thickness of the line, respectively; and Z_C is the characteristic impedance of the microstrip line. Based on empirical calculations, the C per unit length of a 50 Ω transmission line on an FR4 dielectric substrate is about 88.9 pF/mm.

Figure 3 depicts the differential line resistance interconnection topology. The differential line is supposed to cascade numerous times in microwave circuit theory, depending on the number of subcomponents. The difference line's Kron equivalent topological network is displayed in Fig. 3(a); the efficacy of this approach has already been confirmed in prior studies [19–23]. With respect to the interconnection structure, MKM modeling extends the short-circuit terminal network by adding a differential line network (refer to the dotted rectangular box in the figure). The difference lines are then split into equal subnetworks, and the interconnection matrix is created and utilized to

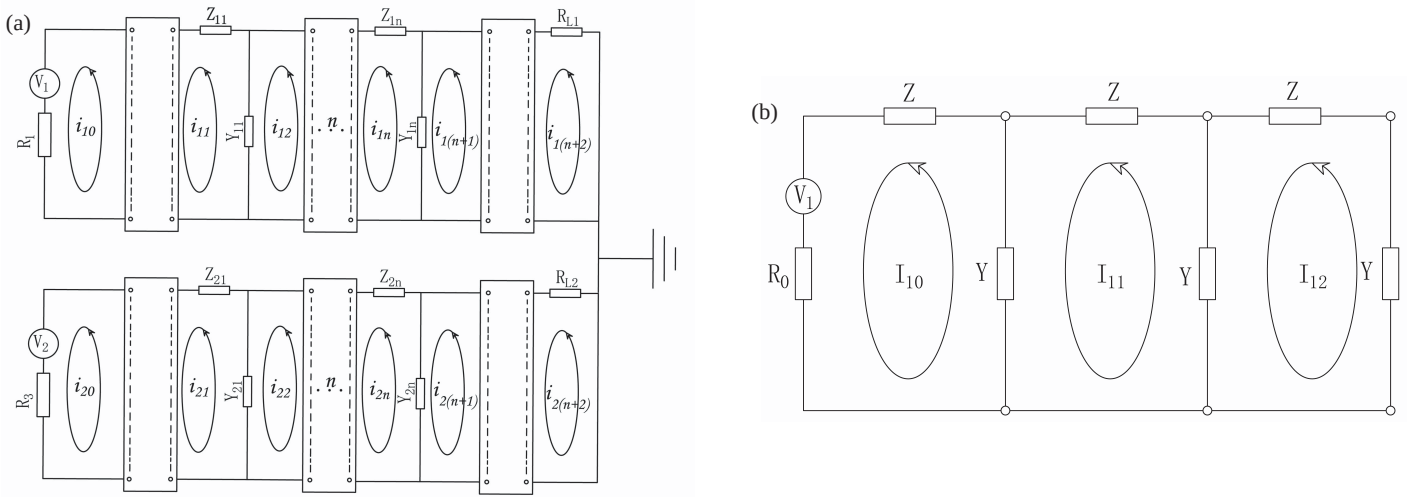

Kron equivalent topology of differential line

topology of single transmission line

FIGURE 3. Topological map.

link each subnetwork. The S scattering parameters are finally computed. A topology diagram for a single transmission line is shown in Fig. 3(b). The voltage excitation and impedance matrix model can be written as follows:

$$[Z] = \begin{bmatrix} R_1 & 0 & 0 \\ 0 & [Z_C] & 0 \\ 0 & 0 & R_L \end{bmatrix} \tag{5}$$

$$[E] = \begin{bmatrix} V_1 & 0 & \ldots & 0 \end{bmatrix} \tag{6}$$

Formula (5) represents the impedance matrix of the difference line. Because the characteristic impedance of the input and output needs to be matched, the impedance matching of the characteristic impedance is $50\,\Omega$, That is, $R = 50\,\Omega$. In Fig. 3(a), i_{11} and i_{12} represent the grid current, and $Z_{1j}\,|_{j=1L(2n-1)}$ and $Y_{1j}\,|_{j=1L(2n-1)}$ are the impedance and admittance of the transmission line per unit length, respectively. According to the grid of i_{11} and i_{12}, the following expressions can be obtained:

$$Z_{11}i_{11} + (i_{11} - i_{12})\frac{1}{Y_{11}} = 0 \tag{7}$$

$$(i_{11} - i_{12})\frac{1}{Y_{11}} = 0 \tag{8}$$

From the above-mentioned two formulas,

$$[e] = [Z_{1j}]\,[i_{1j}] \tag{9}$$

$$[Z_{1j}]_{j=1(2n-1)} = \begin{bmatrix} Z_{11} + \frac{1}{Y_{11}} & -\frac{1}{Y_{11}} \\ \frac{1}{Y_{11}} & -\frac{1}{Y_{11}} \end{bmatrix} \tag{10}$$

Before generating the impedance matrix model of Formula (5), the subnet needs to be connected. A systematic transition is depicted in Fig. 3 from (a) to (b), where (b) is taken from the theory of subnetwork interconnection for a single microstrip line. A connectivity matrix from (a) to (b) and the related grid current function must both be specified to translate the graph into the correct abstract mathematical statement.

$$\begin{cases} i_{10} = 1I_{11} + 0I_{13} + 0I_{15} + \ldots + 0I_{1(n+2)} \\ i_{11} = 1I_{11} + 0I_{13} + 0I_{15} + \ldots + 0I_{1(n+2)} \\ i_{12} = 0I_{11} + 1I_{13} + 0I_{15} + \ldots + 0I_{1(n+2)} \\ i_{13} = 0I_{11} + 1I_{13} + 0I_{15} + \ldots + 0I_{1(n+2)} \\ \vdots \\ i_{1(n+1)} = 0I_{11} + 0I_{13} + 0I_{15} + \ldots + 1I_{1(n+2)} \\ i_{1(n+2)} = 0I_{11} + 0I_{13} + 0I_{15} + \ldots + 1I_{1(n+2)} \end{cases} \tag{11}$$

The relationship between the grid current function I and connectivity matrix F can be found in the transformation between Figs. 3(a) and (b). Subnetworks can be compared to earlier networks because they are all similar to prior subnetworks.

Consequently, the expression that follows can be obtained:

$$\left[i_{1(n+1)}\right] = [F]\left[I_{1(n+1)}\right] \tag{12}$$

The interconnection matrix F is defined as follows:

$$[F] = \begin{bmatrix} 1 & 0 & \cdots & 0 & 0 \\ 1 & 1 & \cdots & 0 & 0 \\ \vdots & 1 & \ddots & 1 & \vdots \\ 0 & 0 & \cdots & 1 & 1 \\ 0 & 0 & \cdots & 0 & 1 \end{bmatrix} \tag{13}$$

Next, the mathematical model of the through-hole was created, along with a computation technique for it. For the two microstrip lines' vias, the same parameters were used. The corresponding modeling topology of a single via on a four-layer plate is displayed in Fig. 4. The following is the formula for calculating the equivalent parameters of the vias:

$$Z_{via} \approx 0.1\sqrt{L_{via}C_{via}} \tag{14}$$

$$C_{via} \approx \frac{\pi\varepsilon_r}{4}\left(\frac{d_2 - t}{\mathrm{In}\frac{d_2 - t}{d_1 + t}} - \frac{d_1 + t}{\mathrm{In}\frac{d_2 - t}{d_1 + t}}\right) \tag{15}$$

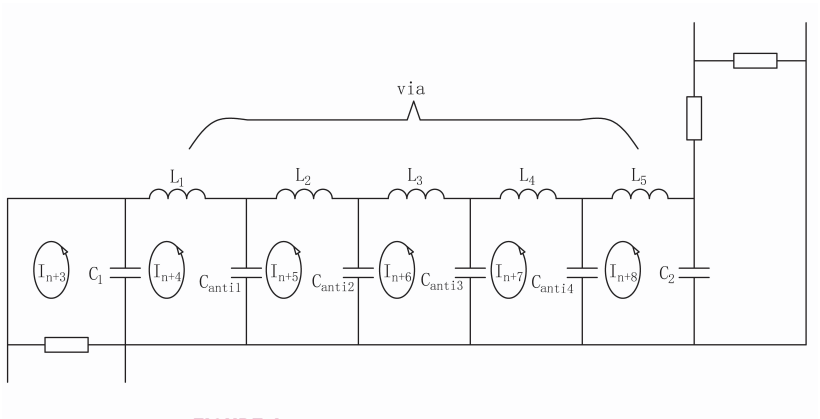

FIGURE 4. Through-hole equivalent topology.

$$L_{via} \approx 0.2h\sqrt{\frac{d_1 d_2}{d_2 - d_1}}\left(\ln\frac{4h}{t}\left(\sqrt{\frac{d_2}{d_1}}+1\right) - \frac{1}{2}\ln\frac{d_2 - t}{d_1 + t}\right) \quad (16)$$

$$Z_{pad} \approx \frac{60}{\sqrt{\varepsilon_r}}\ln\sqrt{\frac{4h}{d}} \quad (17)$$

where L_n and C_{anti} are the equivalent inductance and equivalent capacitance generated by the microstrip line and the hole, respectively, and the units are nh and pF; C_1 and C_2 are equivalent capacitance generated by pad and hole, respectively. Some parameters can be found in Table 1, but when the parameters are substituted into the calculation of formulas (14), (15), (16), and (17), the parameter units need to be converted to inch.

According to formulas (7), (8), (9), the following impedance matrices similar to formula (10) can be obtained. Get the final difference line model. The final impedance matrix can be obtained:

$$[Z] = \begin{bmatrix} R_0 & 0 & \cdots & & 0 & 0 \\ 0 & Z_{11} & \cdots & & 0 & 0 \\ & & \ddots & & & \\ \vdots & \vdots & & Z_{1j} & \vdots & \vdots \\ & & & Z_{via} & & \\ 0 & 0 & \cdots & & Z_{pad} & 0 \\ 0 & 0 & \cdots & & 0 & R_L \end{bmatrix} \quad (18)$$

Figure 4 shows the impedance matrix $[Z']$ and voltage excitation vector $[E']$, which can be determined by the following relationship (20):

$$[E'] = [F]^t [E] \quad (19)$$

$$[Z'] = [F]^t [Z] [F] \quad (20)$$

where $[F]^t$ is the transpose of matrix $[F]$. Then, the following formulas can be obtained:

$$[I] = [Z'] [E'] \quad (21)$$

Finally, scattering parameter S, which represents the relationship between the two ports, is derived. S_{11} is the return loss (RL), which reflects the relationship between the energy emitted by a port and the energy bounced back. In the logarithmic case, the smaller the coefficient is, the better the transmission performance is. S_{11} is the insertion loss (IL), which reflects the relationship between the energy transmitted by one port and the energy received by another port. In the logarithmic case, the greater the coefficient is, the better the transmission performance is. They can be obtained using the grid current as follows:

$$S_{11} = \frac{1 - 2R_0 I_{11}}{V_1} \quad (22)$$

$$S_{21} = \frac{-2R_L I_{1(n+2)}}{V_1} \quad (23)$$

3. SIMULATION AND TEST OF HIGH-SPEED DIFFERENTIAL LINE

3.1. Related Parameter Description

The simulation performed in this study was based on the configuration of a four-layer PCB. The high-speed differential line had a symmetrical structure (i.e., from the left side of the top layer to the middle, then down to the bottom through the pad and via, and finally reaching the rightmost side) [28]. The spacing of the initial model was 0.35 mm; the center of the model's geometry was used to represent the coordinate origin; the center coordinate of the hole was $(0, 0.5, 0)$; and the coordinate of the turning point adjacent to the difference line was $(-0.477, 0.175, 0)$. The frequency of the simulation test was from 0 to 8 GHz. The relevant parameters, such as S parameters and impedance parameters, were extracted from the simulation results. Table 1 shows the parameter design related to the PCB and the differential line. Table 2 shows the laminated structural design of each layer of the PCB. The length parameter is measured in millimeters.

3.2. Initial Model Production Test and Simulation

After HFSS simulation and optimization are completed, the manufacturer is commissioned to process and manufacture the product; considering that the processing will be subject to physical tolerances, the step size is usually set to $\geq$ physical tolerance during the optimization process; and finally an experimental test is performed. For better experimental testing, some

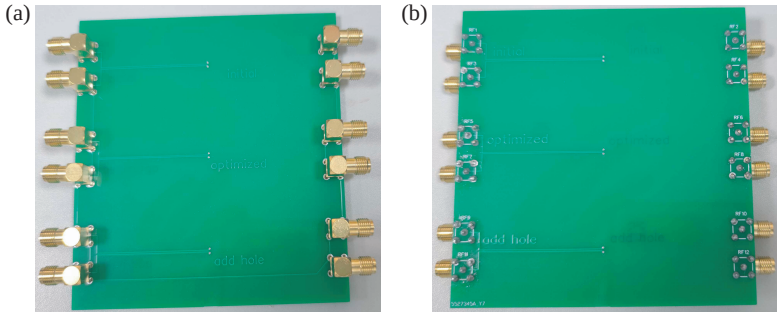

front part of the PCB back part of the PCB

FIGURE 5. Actual picture.

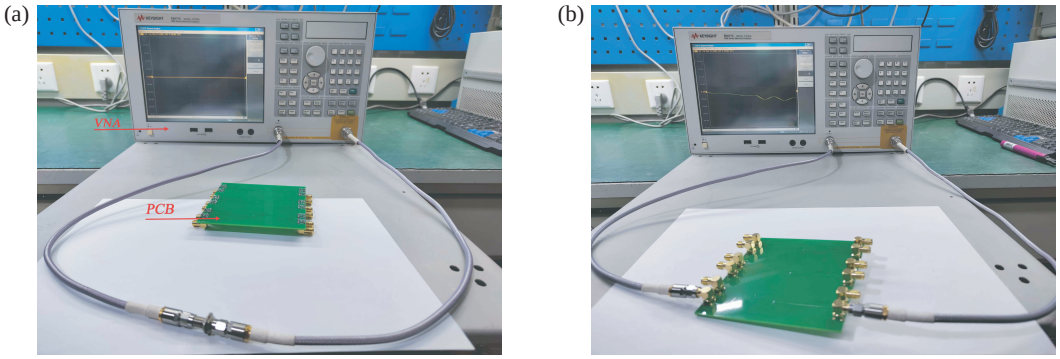

Correction diagram Experimental test diagram

FIGURE 6. Pilot test.

TABLE 1. PCB board and differential line parameters.

Name	Value/mm
PCB length (l)	100
PCB width (w)	100
Microstrip line width (wid)	0.254
Microstrip line thickness (t)	0.035
Differential line spacing (d)	0.35
The inner diameter of the hole (d_1)	0.2
Outside diameter of through (d_2)	0.22
Diameter of pad (d_3)	0.6
Through-hole diameter (d_4)	0.2

TABLE 2. PCB laminated structure design.

Name	Material	Thickness/mm
Top layer	copper	0.035
Medium layer 1	Fr4	0.11
Medium layer 2	copper	0.017
Medium layer 3	Fr4	0.566
Medium layer 4	copper	0.017
Medium layer 5	Fr4	0.11
Medium layer 6	copper	0.017
Medium layer 7	FR4	0.566
Medium layer 8	copper	0.017
Medium layer 9	Fr4	0.11
Bottom layer	copper	0.035

areas are drained next to the difference line to facilitate the installation of SMA connectors. The actual picture is shown in Fig. 5 ((a) front side of the actual picture and (b) back side of the actual picture). Shown in the figures are the actual pictures of the initial, the added through-hole, and the final optimized differential line, respectively. The SMA connector is fixed by solder.

Figure 6(a) shows the self-test schematic of the network analyzer (VNA) and the input and output refluxes to help determine whether the detection device can be used normally, and to ensure that the instrument has no error, or the error can be ignored, and at the same time ensure the scientific and accuracy of the experiment. Meanwhile, it can ensure the accuracy of the experimental equipment. Fig. 6(b) shows a picture of a differential line test scenario using a network analyzer. Because the differential lines are symmetrical structures, it is sufficient to test only one of them. The VNA is connected to the PCB with a welded RF terminal through an SMA connector.

Figure 7 shows the diagram for $d = 0.35$ mm. There are simulation data, test data, and scattering parameter curves of two, four, and eight Kron subnetworks, respectively. The Kron subnetwork data only calculate the values of eight points, and finally the curve is obtained by fitting. Fig. 7(a) illustrates the S_{11} curve of the initial model, in which S_{11} is greater than -5 dB

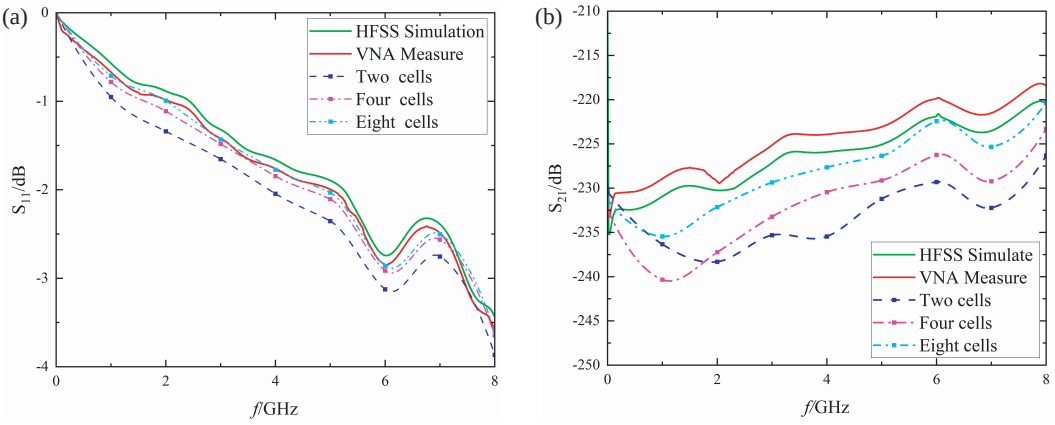

S_{11} parameter curve S_{21} parameter curve

FIGURE 7. S parameter simulation curve of initial model.

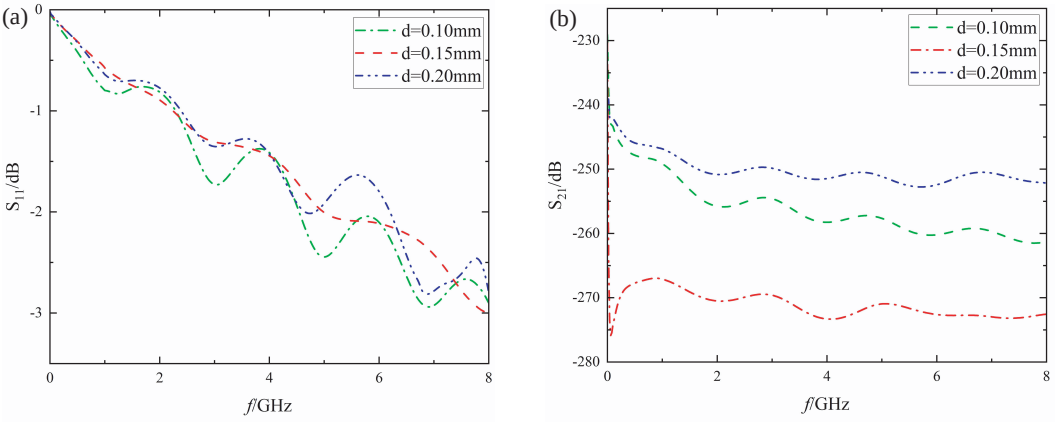

S_{11} parameter curve S_{21} parameter curve

FIGURE 8. S parameter simulation curve of change d.

in the range of 0 to 8 GHz, indicating that the reflection of S_{11} is relatively large, and the transmission effect is not very good. Fig. 7(b) illustrates the S_{21} curve of the initial model, in which S_{21} is less than -215 dB in the range of 0 to 8 GHz, and S_{21} is small, indicating that the forward transmission energy is small, and the transmission performance is poor. The reason for this is that the parameters chosen for the initial model produce poor results, and it can even be said that differential lines with such parameters do not transmit signals, so the following optimizations were made.

3.3. Effect of *d* on the Transmission Characteristics of Differential Lines

With the consideration that through-holes and spacing can have an impact on differential line transmission performance, Figs. 8(a) and (b) show the S_{11} and S_{21} curves for the changed spacing of the initial model, respectively. Without adding through-hole structures, the change in d does not improve the transmission effect of the differential line. The reflection and RL are both large. Meanwhile, the forward transmission is poor, and IL is extremely small.

3.4. Effect of Through-Hole Radius on the Transmission Characteristics of Differential Lines

The coordinates of the through-hole mechanism are $(0, 2, 0)$. As shown in Fig. 9(a), S_{11} is less than -15 dB in general in the range of 0 to 8 GHz. The reflection is small, but RL is much smaller. Fig. 10(b) shows the S_{21} parameter curve. In the range of 0 to 8 GHz, the IL is greater than -3.5 dB, indicating improvements in forward transmission performance. Thus, it is shown that the through-hole structure has the effect of improving signal transmission over the transmission line in this paper.

3.5. The Optimized Model Is Finally Obtained

Given the influence of the above mentioned parameters discussed above, the influences of $d = 0.2$ mm and d_4 were further considered in this study.

As shown in Fig. 10(a), the S_{11} parameter is greater than -15 dB in the range of 0 to 8 GHz. A comparison of this plot with that in Fig. 8 shows that S_{11} has been improved. Meanwhile, in Fig. 10(b), when $d_4 = 0.2$ mm, S_{21} is greater than -3 dB in the range of 0 to 8 GHz. Comparing this plot with that in Fig. 8 indicates an increase in the minimum point by -0.5 dB, and S_{21} is much smoother.

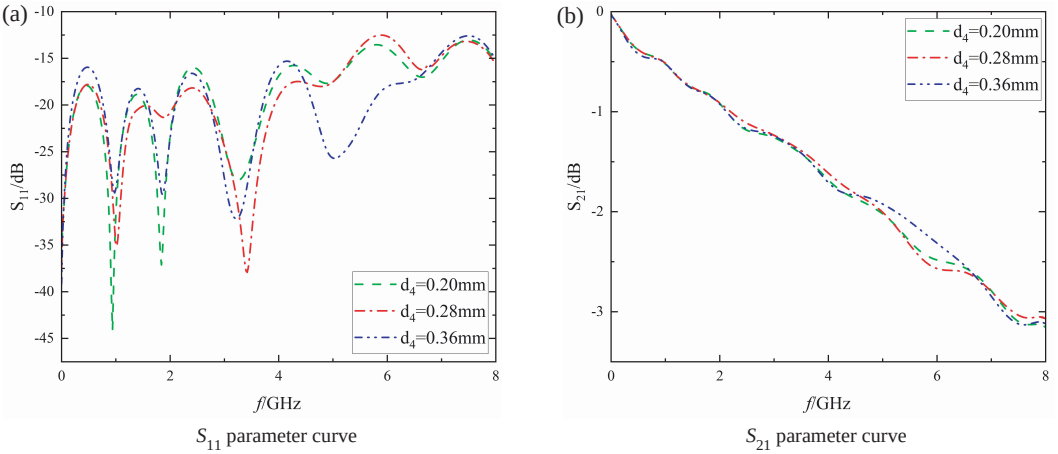

S_{11} parameter curve S_{21} parameter curve

FIGURE 9. S parameter simulation curve of change the through-hole mechanism.

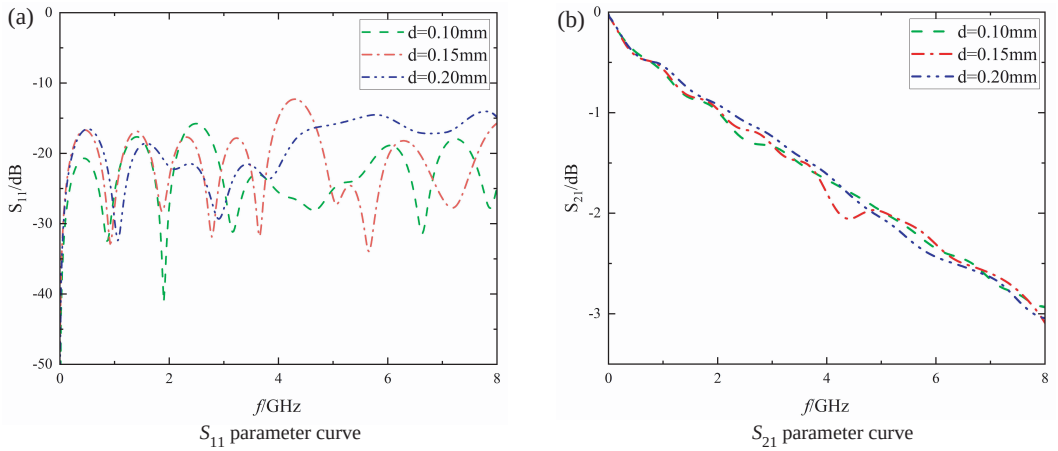

S_{11} parameter curve S_{21} parameter curve

FIGURE 10. Final optimized S parameter simulation curve.

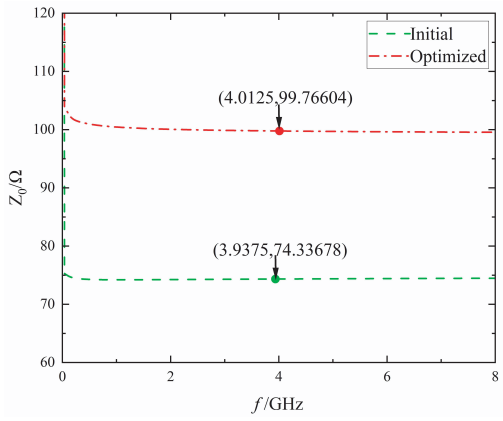

FIGURE 11. Characteristic impedance Z_0 curve.

A comparison of the initial and optimization models indicates that the characteristic impedance of the differential line is also optimal, which matches the port impedance. Fig. 11 shows the characteristic impedance of the Z_0 curve. The initial differential characteristic impedance of the differential line is approximately 74 Ω, and the external impedance of the port is 100 Ω. At this time, if the characteristics do not match, then the signal transmission will manifest a discontinuous phenomenon, and the signal transmission will be hindered. The characteristic impedance of the optimized difference line is optimized from approximately 74 Ω to approximately 99.5 Ω. This finding matches the external impedance of the port. By addressing the signal transmission problem from the source, the probability of crosstalk, resonance, and discontinuity can be jointly reduced.

Figure 12 shows the plots for $d = 0.17$ mm, $d_1 = 0.314$ mm, $d_2 = 0.32$ mm, $d_3 = 0.7$ mm, and $d_4 = 0.314$ mm, and there is a comparison of three types of data, namely Kron subnetwork, simulation, and test data. Fig. 12(a) presents the S_{11} curve of the optimized model. As the frequency increases, S_{11} gradually increases. Fig. 12(b) presents the S_{21} curve of the optimized model. As the frequency increases, S_{21} gradually decreases and is accompanied by a jitter.

3.6. The Influence of Multiple Sets of High-Speed Differential Lines

The influence of the horizontal and vertical multiple sets of differential lines on the transmission of differential lines was

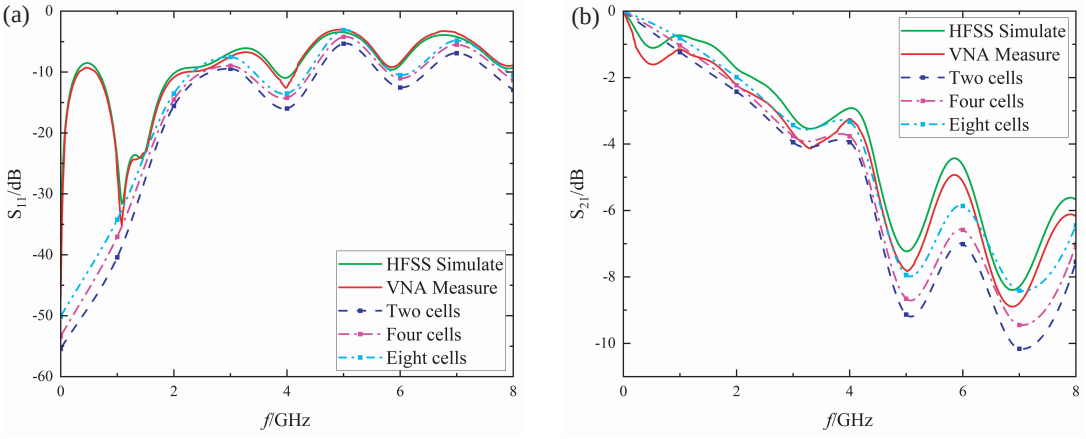

S_{11} parameter curve S_{21} parameter curve

FIGURE 12. Final optimized S parameter simulation curve and is accompanied by a jitter.

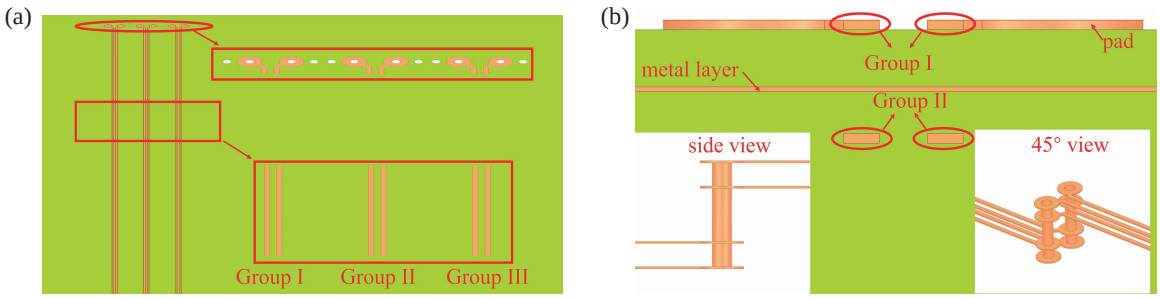

horizontal multi-group difference line model vertical multi-group difference line model

FIGURE 13. Multiple Differential Lines.

investigated. Fig. 13(a) presents the HFSS model diagram of three sets of horizontal differential lines, and the distance between the two sets of horizontal difference lines is $y = 2.5$ mm. Fig. 13(b) shows the HFSS model diagram of two sets of vertical differential lines, and the distance between the two sets of horizontal difference lines is $Z = 0.4$ mm.

As shown in Figs. 14(a) and (b), S_{11} is generally less than -10 dB, while S_{21} is generally greater than -4 dB. These findings indicate that when the multigroup differential lines are horizontally distributed, the effect is negligible, but the transmission effect is substantial. Figs. 14(c) and (d) further show that S_{11} increases with increasing Z, while S_{21} is mostly in the range of -10 to -20 dB. Therefore, the reflection of vertical multiple sets of differential lines is relatively large, and the transmission effect is poor.

Figure 14 shows varying sets of difference lines for distribution. Their comparison indicates that the horizontal distribution is much more conducive to the stability and integrity of the signal.

4. DISCUSSIONS

This work used the FEM technique to the HFSS, which was then utilized to simulate and analyze the high-speed differential lines in a four-layer PCB. The software's precision is more accurate than that of other 3D simulation tools.

Signal transmission jitter was decreased, and S_{11} was smoother when the grounding through-hole structure was enlarged, and the spacing was improved. The transmission loss was decreased by the hole, and the transmission loss may be further decreased by the formation of more grounding vias surrounding the vias. Therefore, the loss resulting from the via hole could be somewhat mitigated by creating a hole surrounding it. The phenomena of parameters S_{11} and Z_0 above are discussed and analyzed as follows:

1. Regarding the influence of different line spacings, the smaller the distance is between the differential lines during high-frequency signal transmission, the greater the influence is caused by coupling, resonance, radiation, and EMI.
2. The discontinuous through-hole impedance, signal integrity, and crosstalk between the differential lines might all are enhanced by the hole structure.
3. The secret to transmitting differential signals is characteristic impedance matching, which allows a signal with a matching impedance to be sent smoothly.
4. Physical tolerances primarily affect the width of the microstrip line and the diameter of the aperture, and indirectly affect the impedance of the microstrip line, thus creating an impedance mismatch problem.

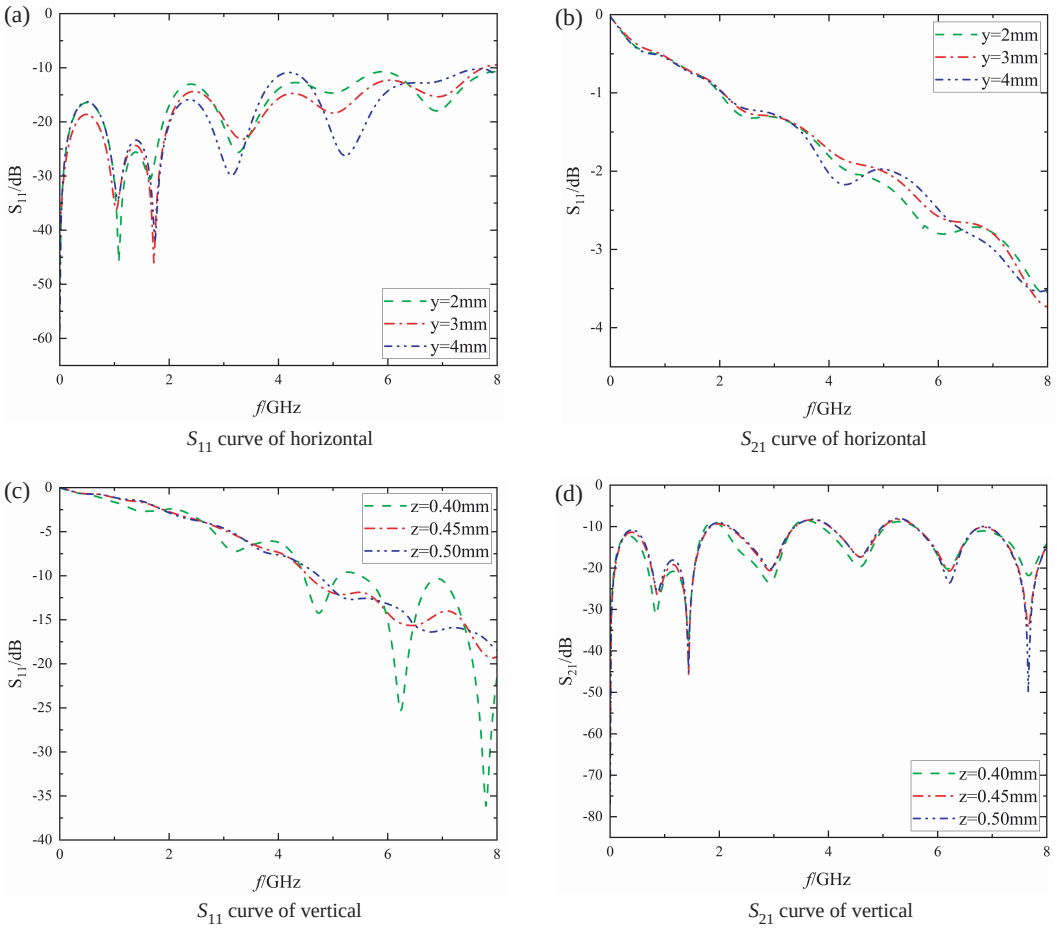

FIGURE 14. Horizontal and vertical S parameter simulation curves.

5. CONCLUSION

A lot of electronic engineers are not familiar with the high-speed differential line model; therefore, this study's analysis of the model produces fresh insights. MKM modeling was used in this study on a four-layer PCB construction using a basic four-layer board model. The TAN model was developed based on it. The modeling procedure and method could also be explained because the suggested model was based on the MKM. In addition, the viability of the differential line-based, four-layer board structure was examined in conjunction with the through-hole structure and pads. From this investigation, the following findings can be drawn:

1. MKM-based modeling is designed to swiftly adapt to extremely complex systems.
2. The quantity of subnetworks affects how accurate MKM modeling is.
3. Grounding vias have a bigger impact on high-speed differential line signal transmission than spacing does.
4. The difference line's horizontal distribution has less impact than its vertical distribution.

It is likely that PCBs will continue to grow in complexity and signal frequency in the future. PCB-EMC models based on Kron's method will be favoured by more and more scholars.

ACKNOWLEDGEMENT

This work was supported in part by the National Natural Science Foundation of China (No. 61763018, 62363014); in part by the Key Project of Natural Science Foundation of Jiangxi Provincial Science and Technology Department under Grant 20232ACB202001; in part by the National 14th Five-Year Plan for Key Research and Development under Grant 2023YFB4302100; in part by the Major Special Project of Jiangxi Provincial Science and Technology Department under Grant 20232ACE01011; in part by the Program of Qingjiang Excellent Young Talents in Jiangxi University of Science and Technology under Grant JXUSTQJBJ2019004; the Research Projects of Ganjiang Innovation Academy, Chinese Academy of Sciences. (No. E255J001).

REFERENCES

[1] Swaminathan, M., D. Chung, S. Grivet-Talocia, K. Bharath, V. Laddha, and J. Xie, "Designing and modeling for power integrity," *IEEE Transactions on Electromagnetic Compatibility*, Vol. 52, No. 2, 288–310, 2010.

[2] Li, E.-P., X.-C. Wei, A. C. Cangellaris, E.-X. Liu, Y.-J. Zhang, M. D'amore, J. Kim, and T. Sudo, "Progress review of electromagnetic compatibility analysis technologies for packages, printed circuit boards, and novel interconnects," *IEEE Transac-*

tions on Electromagnetic Compatibility, Vol. 52, No. 2, 248–265, 2010.

[3] Montrose, M. I., *Printed Circuit Board Design Techniques for EMC Compliance*, IEEE Press Piscataway, NJ, 1996.

[4] Archambeault, B., C. Brench, and S. Connor, "Review of printed-circuit-board level EMI/EMC issues and tools," *IEEE Transactions on Electromagnetic Compatibility*, Vol. 52, No. 2, 455–461, 2010.

[5] Kim, J. and E. Li, "Special issue on PCB level signal integrity, power integrity, and EMC," *IEEE Transactions on Electromagnetic Compatibility*, Vol. 52, No. 2, 246–247, 2010.

[6] Schuster, C. and W. Fichtner, "Parasitic modes on printed circuit boards and their effects on EMC and signal integrity," *IEEE Transactions on Electromagnetic Compatibility*, Vol. 43, No. 4, 416–425, 2001.

[7] Fan, J., X. Ye, J. Kim, B. Archambeault, and A. Orlandi, "Signal integrity design for high-speed digital circuits: Progress and directions," *IEEE Transactions on Electromagnetic Compatibility*, Vol. 52, No. 2, 392–400, 2010.

[8] Yasunaga, M., H. Shimada, K. Seki, and I. Yoshihara, "Segmental transmission line: Its practical application the optimized pcb trace design using a genetic algorithm," in *2014 IEEE International Conference on Evolvable Systems*, 23–30, Orlando, FL, USA, 2014.

[9] Takamatsu, K., T. Tobana, Y. Isota, and T. Sasamori, "Analysis of transmission characteristic of a microstrip line placed above a ground slot," in *2016 International Symposium on Electromagnetic Compatibility — EMC EUROPE*, 94–99, Wroclaw, Poland, 2016.

[10] Yasunaga, M., Y. Kuribara, H. Inoue, and I. Yoshihara, "Simultaneous improvement to signal integrity and electromagnetic interference in high-speed transmission lines," in *2015 IEEE Symposium Series on Computational Intelligence*, 1236–1243, Cape Town, South Africa, 2015.

[11] Xie, W., S. Mei, H. Wang, and H. Zhang, "A digital system design of high-speed acquisition module," in *2021 IEEE 3rd International Conference on Circuits and Systems (ICCS)*, 15–18, Chengdu, China, 2021.

[12] Vouvakis, M. N. and J. Moshfegh, "Sparse direct matrix solvers of finite element discretizations in electromagnetics," in *2018 International Applied Computational Electromagnetics Society Symposium (ACES)*, 1–2, Denver, CO, USA, 2018.

[13] Laour, M., R. Tahmi, and C. Vollaire, "Experimental evaluation and fdtd method for predicting electromagnetic fields in the near zone radiated by power converter systems," *Turkish Journal of Electrical Engineering and Computer Sciences*, Vol. 25, No. 2, 1460–1471, 2017.

[14] Jiao, D., M. Lu, E. Michielssen, and J.-M. Jin, "A fast time-domain finite element-boundary integral method for electromagnetic analysis," *IEEE Transactions on Antennas and Propagation*, Vol. 49, No. 10, 1453–1461, 2001.

[15] Baek, S., S. Ahn, J. Park, J. Kim, J. Kim, and J.-H. Cho, "Accurate high frequency lossy model of differential signal line including mode-conversion and common-mode propagation effect," in *2004 International Symposium on Electromagnetic Compatibility (IEEE Cat. No.04CH37559)*, Vol. 2, 562–566, Silicon Valley, CA, USA, 2004.

[16] Rao, C. S. S., S. Tunga, and A. Kumar, "Analysis of high speed design on a multilayer PCB substrate," in *2021 International Conference on Recent Trends on Electronics, Information, Communication & Technology (RTEICT)*, 713–717, Bangalore, India, 2021.

[17] Kron, G., "Diakoptics-a gateway into universal engineering," *Electrical Journal (London)*, Vol. 157, 1940–1945, 1956.

[18] Maurice, O., A. Reineix, P. Durand, and F. Dubois, "Kron's method and cell complexes for magnetomotive and electromotive forces," *ArXiv Preprint ArXiv:1412.0187*, 2014.

[19] Ravelo, B., O. Maurice, and S. Lalléchère, "Asymmetrical 1:2 Y-tree interconnects modelling with Kron-Branin formalism," *Electronics Letters*, Vol. 52, No. 14, 1215–1216, 2016.

[20] Leman, S., "Contribution à la résolution de problèmes de compatibilité électromagnétique par le formalisme des circuits électriques de Kron," Ph.D. dissertation, Université Polytechnique Hauts-de-France, Valenciennes, France, 2009.

[21] Maurice, O., "Modified Kron's method for electromagnetic compatibility-MKME-an abstract," *Rapport Technique*, May 2007.

[22] Ravelo, B. and O. Maurice, "Kron-Branin modeling of YY-tree interconnects for the PCB signal integrity analysis," *IEEE Transactions on Electromagnetic Compatibility*, Vol. 59, No. 2, 411–419, 2016.

[23] Xu, Z., B. Ravelo, O. Maurice, J. Gantet, and N. Marier, "Radiated EMC Kron's model of 3-D multilayer pcb aggressed by broadband disturbance," *IEEE Transactions on Electromagnetic Compatibility*, Vol. 62, No. 2, 406–414, 2019.

[24] Huang, S. and L. Tsang, "Fast broadband modeling of traces connecting vias in printed circuit boards using broadband Green's function method," *IEEE Transactions on Components, Packaging and Manufacturing Technology*, Vol. 7, No. 8, 1343–1355, 2017.

[25] Xu, Z., Y. Liu, B. Ravelo, and O. Maurice, "Multilayer power delivery network modeling with modified Kron's method (MKM)," in *2017 International Symposium on Electromagnetic Compatibility — EMC EUROPE*, 1–6, Angers, France, 2017.

[26] Rogard, E., B. Azanowsky, and M. M. Ney, "Comparison of radiation modeling techniques up to 10 GHz — Application on a microstrip PCB trace," *IEEE Transactions on Electromagnetic Compatibility*, Vol. 52, No. 2, 479–486, 2010.

[27] Xu, Z., Y. Liu, B. Ravelo, and O. Maurice, "Modified Kron's TAN modeling of 3D multilayer PCB," in *2017 11th International Workshop on the Electromagnetic Compatibility of Integrated Circuits (EMCCompo)*, 224–229, St. Petersburg, Russia, 2017.

[28] Mbairi, F. D., W. P. Siebert, and H. Hesselbom, "High-frequency transmission lines crosstalk reduction using spacing rules," *IEEE Transactions on Components and Packaging Technologies*, Vol. 31, No. 3, 601–610, 2008.